The Astrophysical Journal, 759:119 (12pp), 2012 November 10 doi:10.1088/0004-637X/759/2/119

A DISK-BASED DYNAMICAL MASS ESTIMATE FOR THE YOUNG BINARY V4046 Sgr

Katherine A. Rosenfeld[1], Sean M. Andrews[1], David J. Wilner[1], and H. C. Stempels[2]
[1] Harvard-Smithsonian Center for Astrophysics, 60 Garden Street, Cambridge, MA 02138, USA
[2] Department Physics and Astronomy, Uppsala University, Box 516, SE-751 20 Uppsala, Sweden
Received 2012 July 20; accepted 2012 September 12; published 2012 October 26

ABSTRACT

We present sensitive, arcsecond-resolution Submillimeter Array observations of the ^{12}CO $J = 2$–1 line emission from the circumstellar disk orbiting the double-lined spectroscopic binary star V4046 Sgr. Based on a simple model of the disk structure, we use a novel Monte Carlo Markov Chain technique to extract the Keplerian velocity field of the disk from these data and estimate the total mass of the central binary. Assuming the distance inferred from kinematic parallax measurements in the literature ($d \approx 73$ pc), we determine a total stellar mass $M_* = 1.75^{+0.09}_{-0.06}\ M_\odot$ and a disk inclination $i_d = 33.^\circ5^{+0.7}_{-1.4}$ from face-on. These measurements are in excellent agreement with independent dynamical constraints made from multi-epoch monitoring of the stellar radial velocities, confirming the absolute accuracy of this precise (∼few percent uncertainties) disk-based method for estimating stellar masses and reaffirming previous assertions that the disk and binary orbital planes are well aligned (with $|i_d - i_*| \approx 0.^\circ1 \pm 1^\circ$). Using these results as a reference, we demonstrate that various pre-main-sequence evolution models make consistent and accurate predictions for the masses of the individual components of the binary, and uniformly imply an advanced age of ∼5–30 Myr. Taken together, these results verify that V4046 Sgr is one of the precious few nearby and relatively evolved pre-main-sequence systems that still hosts a gas-rich accretion disk.

Key words: protoplanetary disks – stars: individual (V4046 Sgr)

Online-only material: color figures

1. INTRODUCTION

Mass is the fundamental property that sets the evolutionary path of a star. The masses of young stars are of particular interest in many astrophysical problems: they provide unique information about the star formation process (e.g., accretion histories, the initial mass function; see Bastian et al. 2010) and are thought to have a substantial influence on the evolution of their circumstellar material, and therefore the efficiency of the planet formation process (e.g., see Alibert et al. 2011). Unfortunately, measurements of pre-main-sequence (pre-MS) star masses are difficult and accordingly rare. Unlike their more evolved counterparts, the location of a young star in the Hertzsprung–Russell (H-R) diagram does not provide a robust estimate of M_* (Hillenbrand & White 2004). The theoretical models for stellar evolution at these early stages are plagued with uncertainties related to rotation (Siess & Livio 1997; Mendes et al. 1999), accretion (Siess et al. 1997; Baraffe et al. 2009; Baraffe & Chabrier 2010), magnetic fields (D'Antona et al. 2000), atmosphere properties (e.g., convection, opacities; Baraffe et al. 2002), and unknown initial conditions. Ultimately, a more nuanced understanding of star and planet formation requires pre-MS evolution models that are empirically calibrated with direct, independent, and accurate M_* measurements.

The only *direct* methods available for measuring stellar masses are based on orbital dynamics. In sufficiently close pre-MS binary star systems, M_* can be estimated from the stellar orbits using multi-epoch radial velocity (RV) measurements (e.g., Mathieu et al. 1989, 1991, 1997) and/or long-term astrometric monitoring (Tamazian et al. 2002; Schaefer et al. 2003, 2006; Duchêne et al. 2006). For a double-lined spectroscopic binary (SB2), the RV method provides a robust estimate of $M_*(\sin i_*)^3$ for each component, where i_* is the inclination angle of the orbit projected on the sky. For "visual" binaries, the astrometric monitoring technique offers a constraint on the quantity $M_{\rm tot}d^3$, where $M_{\rm tot}$ is the sum of the stellar masses and d is the distance to the binary. Generally, the stellar mass estimates from these methods are inherently uncertain due to their strong dependences on the unknown values of i_* or d. The $\{M_*, i_*\}$ degeneracy is broken for the special case of an eclipsing SB2, but few pre-MS systems with such favorable orientations are known (e.g., Stassun et al. 2004; Morales-Calderón et al. 2012, and references therein). In a subset of ideal cases, the RV and astrometric techniques can be combined to alleviate the uncertainties related to $\{i_*, d\}$ and extract accurate M_* values (e.g., Steffen et al. 2001; Schaefer et al. 2008; Boden et al. 2005, 2007, 2009, 2012).

These standard methods are only applicable for binary stars with a narrow range of orbital separations. Alternatively, for any *isolated* young star with a circumstellar disk, M_* can be determined from a single millimeter-wave interferometric observation of an optically thick emission line (with a linear dependence on d). This latter technique relies on modeling the spatially and spectrally resolved Keplerian rotation curve of the molecular gas disk that orbits the young star (Koerner et al. 1993; Dutrey et al. 1994, 1998; Simon et al. 2000). While this method has extraordinary value in its more general applicability, it has only been successfully employed for small samples. Attempts to expand its reach have been frustrated by molecular cloud contamination and observational limitations in resolution and sensitivity. Moreover, a reconstruction of the disk velocity field necessarily involves fitting such data with a relatively complicated model of the disk structure (Beckwith & Sargent 1993). Given that added complexity, there is naturally some concern about the absolute accuracy of the M_* estimates from this method (e.g., Gennaro et al. 2012), despite the impressive formal precision of the measurements (∼2%–3%; e.g., Piétu et al. 2007).

The young binary V4046 Sgr provides a rare opportunity to benchmark the disk kinematics method for estimating M_* against the more traditional RV technique for an SB2 system. V4046 Sgr is a nearly equal mass ($q \approx 0.94$) pair of solar-type

pre-MS stars in a circular ($e \leqslant 0.01$), non-eclipsing orbit with a 2.4 day period ($a \sin i_* \approx 5.1\ R_\odot$; Byrne 1986; Quast et al. 2000; Stempels & Gahm 2004). The system is completely isolated from any known molecular clouds and has been kinematically associated with the ∼8–20 Myr old β Pic moving group; a moving cluster analysis suggests it is relatively nearby, $d = 73$ pc (Torres et al. 2006). Despite its advanced age, V4046 Sgr hosts a large and massive circumbinary disk that exhibits a rich molecular emission line spectrum (Kastner et al. 2008; Rodriguez et al. 2010; Öberg et al. 2011). Since the binary orbit is tight and circular, it has no dynamical impact on the disk structure outside a radius of ∼0.1 AU (e.g., see Artymowicz & Lubow 1994). With its central SB2 host, rare proximity to the Sun, lack of molecular cloud contamination, and intrinsically bright, spatially extended line emission, the V4046 Sgr disk is an ideal target to assess the accuracy of the disk kinematics technique for measuring M_*.

In this article, we build on some initial work by Rodriguez et al. (2010) and use high-quality spatially and spectrally resolved observations of the CO $J = 2$–1 emission line to measure the velocity field of the V4046 Sgr disk and extract the total mass of the close binary at its center. Our millimeter-wave observations with the Submillimeter Array (SMA) and data calibration procedures are described in Section 2. A detailed overview of the modeling analysis is provided in Section 3. The modeling results are presented and compared with the complementary RV analysis of the central SB2 by H. C. Stempels (2012, in preparation) in Section 4. These results are discussed in the context of the V4046 Sgr system in particular, pre-MS evolution models more generally, and future prospects for M_* estimates from the disk kinematics method in Section 5. Some key conclusions from this work are summarized in Section 6.

2. OBSERVATIONS AND DATA REDUCTION

The V4046 Sgr circumbinary disk was observed at 225 GHz (1.3 mm) with SMA (Ho et al. 2004) on four occasions starting in 2009, using each of the available antenna configurations: subcompact (baseline lengths of 9–25 m; 2011 March 18), compact (16–70 m; 2009 April 25), extended (28–226 m; 2009 February 23), and very extended (68–509 m; 2011 September 4). The SMA double sideband receivers were tuned to simultaneously observe the $J = 2$–1 transitions of ^{12}CO, ^{13}CO, and C^{18}O at 230.538, 220.399, and 219.560 GHz, respectively, and the adjacent dust continuum. The correlator was configured to place those emission lines in separate 104 MHz spectral chunks and sample them finely with 512 channels per chunk, corresponding to a native velocity resolution of ∼0.25 km s^{-1}. The continuum was observed with a more coarse frequency sampling (in 3.25 MHz channels), with a total bandwidth of 1.6 and 3.6 GHz in 2009 and 2011, respectively. The observations cycled between V4046 Sgr and the quasars J1924-292 (15° away) and J1733-130 (22° from V4046 Sgr, 30° from J1924-292) with a total loop time of 10–20 minutes. The bright quasars 3C 84 and 3C 454.3 were also observed as bandpass calibrators, along with Uranus, Callisto, and Ceres for use in determining the absolute scaling of the amplitudes. All of the data were collected in outstanding weather conditions for this observing frequency, with an atmospheric zenith optical depth of only ∼0.05 (corresponding to a precipitable water vapor level of ∼1.0 mm).

Each individual data set was calibrated independently with the MIR software package. The bandpass response was corrected based on observations of bright quasars, and broadband continuum channels were generated from the central portions of all line-free spectral chunks. The visibility amplitude scale was derived by bootstrapping the gain calibrator (quasar) flux densities from the observations of Uranus, Callisto, or Ceres, with a systematic uncertainty estimated at 10%–15%. The antenna-based complex gain response of the system was determined with reference to J1924-292, and the quality of the phase transfer was assessed using the observations of J1733-130. That comparison suggests only a small amount of "seeing" (∼0.″1) was introduced by atmospheric phase noise (or small baseline errors), consistent with the excellent observing conditions. After applying the appropriate (and small) phase shifts to account for the V4046 Sgr proper motion ($\mu_\alpha \cos\delta = 0.''003$ yr^{-1}, $\mu_\delta = -0.''052$ yr^{-1}; Zacharias et al. 2010) and confirming that the continuum amplitudes from different array configurations were consistent on overlapping baseline lengths, the visibility data sets from each observation were combined. The observations of the dust continuum and CO isotopologue emission will be presented in a separate article; the focus here will be solely on the ^{12}CO $J = 2$–1 emission. Note that although the 2009 data were originally presented by Rodriguez et al. (2010), those data have been re-calibrated here for consistency (and modest improvements).

The CO visibilities were continuum subtracted and truncated outside a projected baseline length of 200 kλ to reduce the data volume and improve the signal-to-noise ratio. They were then Fourier inverted, deconvolved with the CLEAN algorithm, and restored with a synthesized beam using the MIRIAD package. The naturally weighted spectral images shown as channel maps in Figure 1 were synthesized on a 0.4 km s^{-1} smoothed velocity scale with a $1.''55 \times 1.''29$ beam (at a position angle of 24°). The typical rms noise level in each channel is 70 mJy beam^{-1}. There is CO emission firmly detected ($>3\sigma$) out to ±4.8 km s^{-1} from the systemic velocity, estimated to be v(LSR) = +2.87 ± 0.05 km s^{-1} (corresponding to −6.26 ± 0.05 km s^{-1} in the heliocentric frame), with an integrated intensity of 27.7 ± 2.8 Jy km s^{-1} and a peak flux density of 1.48 ± 0.16 Jy beam^{-1} (17 ± 2 K; a peak S/N = 21), including the calibration uncertainties. Figure 2 shows a map of the velocity-integrated CO intensities (zeroth moment; *contours*) overlaid on the intensity-weighted velocities (first moment; *color scale*), as well as a spatially integrated CO spectrum. These data exhibit a molecular gas disk with a clear rotation pattern, from east (blueshifted) to west (redshifted), and suggest a modest inclination angle to the line of sight. Near the systemic velocity, the CO emission subtends ∼5″ in radius (∼365 AU; see Rodriguez et al. 2010).

3. MODELING ANALYSIS

The fundamental goal here is to derive a dynamical estimate of the central stellar mass based on the kinematic properties of the V4046 Sgr gas disk. In order to extract M_* from a measurement of the disk velocity field, we need to construct a detailed physical model of the disk structure.[3] We adopt a modeling formalism motivated by Beckwith & Sargent (1993), which makes three basic assumptions about disk properties. First, the disk material is assumed to be orbiting in Keplerian rotation around a point mass, meaning the central stars are treated as one object that dominates the disk velocity field. Previous work has found little evidence to support (simple parametric) deviations from

[3] For the sake of convenient and general notation, we will refer to the central stellar mass as M_*. In this particular case, M_* corresponds to the sum of the stellar masses in the V4046 Sgr binary.

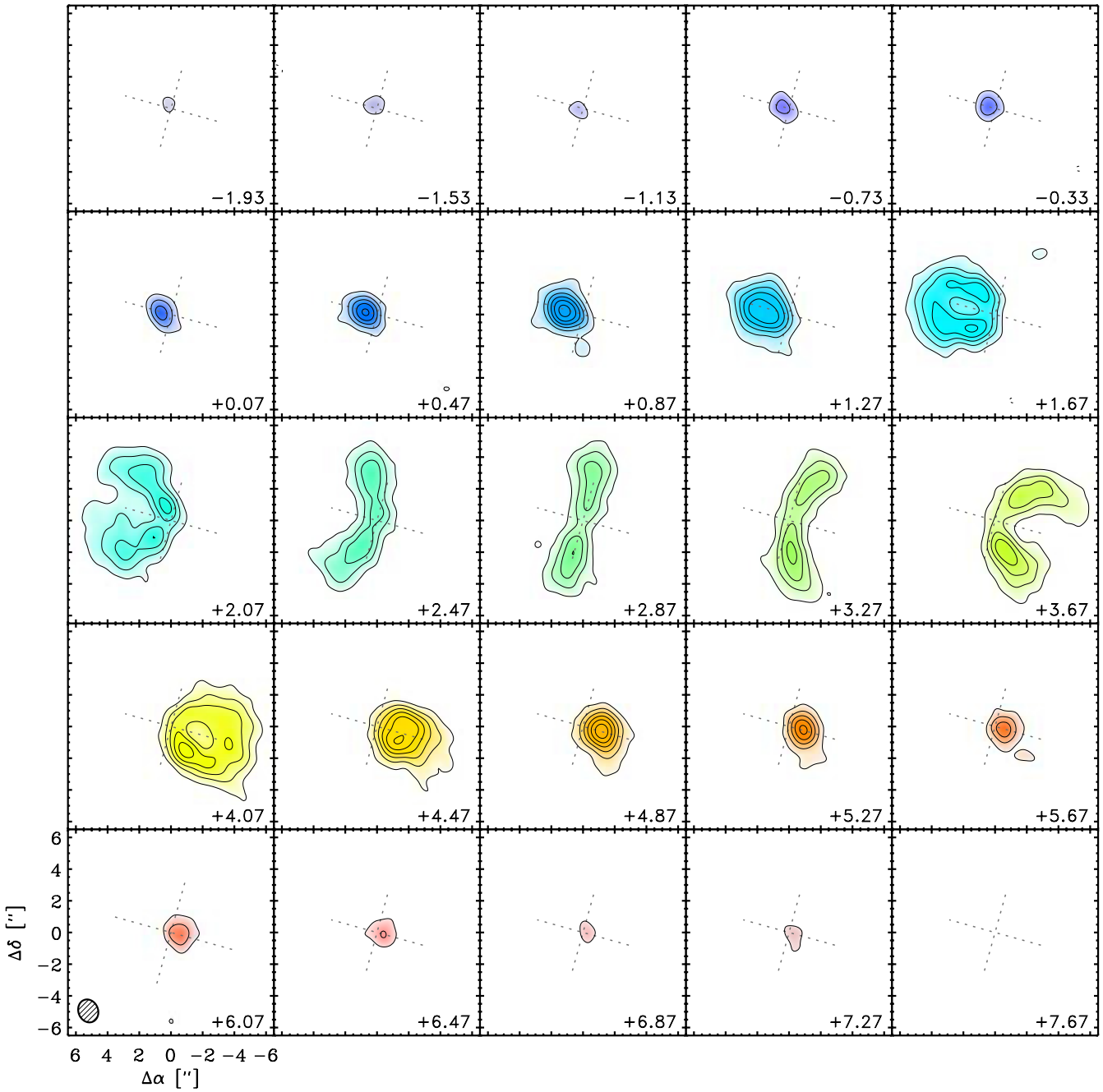

Figure 1. Naturally weighted channel maps of ^{12}CO $J = 2$–1 emission from the V4046 Sgr disk. The synthesized beam dimensions are marked in the bottom left. In each 0.4 km s^{-1} wide channel (LSR velocities labeled in the lower right corner of each panel), contours are drawn at 0.21 Jy beam^{-1} (3σ) intervals, starting at 0.18 Jy beam^{-1}. A linear color scale represents the mean velocity of each channel, with red and blue denoting receding and approaching velocities, respectively.

(A color version of this figure is available in the online journal.)

Keplerian v-fields in disks (e.g., see Simon et al. 2000); the corollary criterion that the disk mass is only a small fraction of the stellar mass ($M_d/M_* \ll 1$) can be confirmed a posteriori (see Section 4). Second, the disk is assumed to be geometrically thin at all radii. Although Piétu et al. (2007) argued that this may not be valid at very large radii (>800 AU), the higher M_* for the V4046 Sgr binary (which decreases the disk scale height; see below) and the limited extent of the CO emission from its disk (<400 AU) suggest it is a reasonable approximation in this case. And third, in the context of the disk structure, we assume that the gas is vertically isothermal and in hydrostatic pressure equilibrium. A more realistic model would include a temperature inversion (e.g., D'Alessio et al. 1998). However, excluding that kind of added complexity does not diminish the accuracy of an M_* estimate: the emission from a single CO line is generated in a narrow vertical layer of the disk atmosphere, which has a roughly constant temperature (Dartois et al. 2003).

The model for the gas density distribution is constructed in cylindrical coordinates (r, ϕ, z),

$$\rho(r, z) = \frac{\Sigma}{\sqrt{2\pi}H_p} \exp\left[-\frac{1}{2}\left(\frac{z}{H_p}\right)^2\right], \quad (1)$$

where Σ is the radial surface density profile and H_p is the pressure scale height at each radius. We assume a parametric version of the former that is appropriate for an accretion disk with a

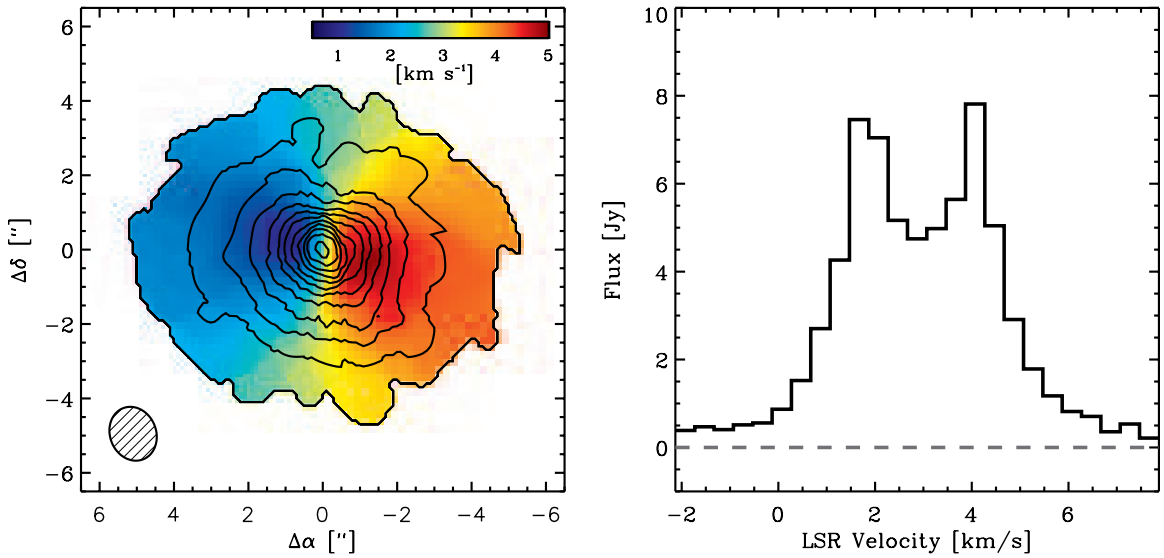

Figure 2. Left: the CO $J = 2$–1 moment maps for the V4046 Sgr disk, on the same angular scale as in Figure 1. The zeroth moment (velocity-integrated intensity) map is overlaid in contours shown at 5σ intervals (0.35 Jy km s^{-1} beam^{-1}), starting at the 3σ level (0.21 Jy km s^{-1} beam^{-1}). The first moment (intensity-weighted velocities) map is shown in color, with a scale bar for reference. Right: the integrated CO $J = 2$–1 line profile from the V4046 Sgr disk, constructed from a square box 10″ on a side centered at the stellar position, and assuming a 2σ threshold for inclusion.

(A color version of this figure is available in the online journal.)

static, power-law viscosity profile (Lynden-Bell & Pringle 1974; Hartmann et al. 1998) and is currently the basis for most dust-based disk density measurements (e.g., Andrews et al. 2009, 2010),

$$\Sigma = \Sigma_c \left(\frac{r}{r_c}\right)^{-\gamma} \exp\left[-\left(\frac{r}{r_c}\right)^{2-\gamma}\right], \quad (2)$$

where γ is a density gradient, r_c is a characteristic radius, and Σ_c is a normalization equivalent to $e \cdot \Sigma(r_c)$. The scale heights are calculated with the explicit assumption of hydrostatic equilibrium and a constant vertical temperature profile, such that

$$H_p = \frac{c_s}{\Omega} = \left(\frac{kT}{\mu m_{\rm H}} \cdot \frac{r^3}{GM_*}\right)^{1/2}, \quad (3)$$

where c_s is the sound speed, Ω is the angular velocity, T is the radial temperature profile, k is the Boltzmann constant, G is the gravitational constant, $m_{\rm H}$ is the mass of a hydrogen atom, and $\mu = 2.37$ is the mean molecular weight of the gas. We further assume a simple power-law behavior for the radial temperature profile,

$$T = T_{10}\left(\frac{r}{10\ {\rm AU}}\right)^{-q}, \quad (4)$$

where q is a temperature gradient and T_{10} is the gas temperature at a radius of 10 AU. The parametric descriptions in Equations (1)–(4) completely characterize the temperature and density structure of a model gas disk. The gas kinematics are described by a Keplerian velocity field,

$$v_\phi(r) = v_k = \sqrt{\frac{GM_*}{r}}; \quad v_r = v_z = 0, \quad (5)$$

meaning there is only rotation, and no net motion in the radial or vertical dimensions.

Given a physical disk structure, we can construct a model of the CO $J = 2$–1 emission with the added assumption that the energy levels relevant for this transition are populated according to local thermodynamic equilibrium (LTE). Although the LTE approximation is not always valid in protoplanetary disks, Pavlyuchenkov et al. (2007) demonstrated that it is an appropriate simplification for the low energy and high optical depths associated with this particular species and transition. We model the emission line intensity distribution by integrating the radiative transfer equation along each sight line s, so that

$$I_\nu = \int_0^\infty K_\nu(s) S_\nu(s) e^{-\tau_\nu(s)} ds, \quad (6)$$

where $K_\nu(s)$ is the absorption coefficient, $S_\nu(s) = B_\nu(T)$ is the source function (here equivalent to the Planck function), and $\tau_\nu(s) = \int_0^s K_\nu(x)dx$ is the optical depth along the line of sight. The absorption coefficient is the sum of contributions from dust and gas. For the former, we assume $K_\nu(s)_{\rm dust} = \rho(s)\,\zeta\,\kappa_\nu$, where the dust-to-gas mass ratio is $\zeta = 0.01$ and the grain opacity is $\kappa_\nu \approx (\nu/100\ {\rm GHz})\ {\rm cm^2\ g^{-1}}$ (Beckwith et al. 1990). In the particular case of the V4046 Sgr disk, the contribution of dust to the absorption coefficient is effectively negligible compared to the gas; the specific choices of ζ and κ_ν (within reasonable limitations) have no tangible effect on our results (moreover, continuum emission is removed from the data before our modeling analysis).

The absorption coefficient of the CO gas is calculated from the transition cross section weighted by the population of the lower energy level, ℓ, such that $K_\nu(s)_{\rm co} = n_\ell(s)\sigma_\nu(s)$ (note that in this specific case, $\ell = 1$). Since we assume that the line is thermally populated in LTE, the level populations are determined by the local disk temperature via the Boltzmann equation,

$$n_\ell(s) = \frac{X_{\rm co}\,\rho(s)}{\mu {\rm m_H}} \cdot \frac{g_\ell}{Z} \exp\left(-\frac{E_\ell}{kT(s)}\right), \quad (7)$$

where E_ℓ is the transition energy, $g_\ell = 2\ell + 1$ is the statistical weight, Z is the partition function, and $X_{\rm co}$ is the CO fractional abundance (assumed to be constant everywhere in the disk). The details of the emission line model are encoded in the absorption

cross section,

$$\sigma_\nu(s) = \phi_\nu(s) \cdot \sigma_0(1 - e^{-h\nu/kT(s)}), \quad (8)$$

where ϕ_ν is the line profile function and the integrated cross section is

$$\sigma_0 = \frac{h\nu}{4\pi} \cdot \frac{g_{\ell+1}}{g_\ell} B_{21} = \frac{c^2}{8\pi\nu^2} \cdot \frac{g_{\ell+1}}{g_\ell} A_{21}, \quad (9)$$

where we have used the Einstein relation in the last equality to express the Einstein-B coefficient in terms of the Einstein-A coefficient provided by the LAMDA molecular database (Schöier et al. 2005). The line profile function naturally determines the shape of the emission line, where a given frequency ν corresponds to an intrinsic Doppler velocity $v_d = (c/\nu_0)(\nu - \nu_0)$ relative to the line center, ν_0. The gas in a given disk model has a projected, line-of-sight velocity field given by $v_{\rm obs} \approx v_\phi(r) \cos\phi \sin i_d$, where i_d is the inclination of the disk relative to the observer (such that $i_d = 90^\circ$ is edge-on; for the geometry, see Isella et al. 2007). The line profile shape at each frequency is determined by the difference between the Doppler and line-of-sight velocities,

$$\phi_\nu(s) = \frac{c}{\sqrt{\pi}\nu_0\Delta v} \exp\left[-\left(\frac{v_d - v_{\rm obs}}{\Delta v}\right)^2\right], \quad (10)$$

and the effective line width, Δv. The latter is comprised of the quadrature sum of contributions from thermal and non-thermal broadening terms,

$$\Delta v = \left(\frac{2kT(s)}{m_{\rm co}} + \xi^2\right)^{1/2}, \quad (11)$$

where $m_{\rm co}$ is the mean molecular weight of CO and ξ is the contribution from microturbulence. We assume that the turbulent velocity width ξ is constant throughout the disk.

The Beckwith & Sargent (1993) model formalism highlighted above is admittedly complex. A single model is completely described by 14 parameters: four quantify the distribution of CO densities $\{X_{\rm co}, \Sigma_c, R_c, \gamma\}$, two characterize the temperature structure (and therefore the vertical density structure) $\{T_{10}, q\}$, three play pivotal roles describing the disk kinematics $\{M_*, \xi, \nu_0\}$, and the remaining five relate the model to the observations—i.e., convert from physical coordinates in the disk to the observed plane projected on the sky—including the disk inclination and major axis position angle $\{i_d, {\rm PA}_d\}$, distance $\{d\}$, and disk center $\{\alpha_0, \delta_0\}$. Some of these parameters can be reliably determined in a simple way, and then fixed to facilitate the data modeling problem (with no tangible impact on the quality of the M_* determination). In this case, the systemic LSR velocity (effectively ν_0) was measured directly from the SMA data and set to $v_0 = +2.87$ km s^{-1}. The disk center coordinates were estimated from both the dust continuum and CO emission morphology at the systemic velocity (see Figure 1) and set to $\alpha_0 = 18^{\rm h}14^{\rm m}10\overset{\rm s}{.}48$, $\delta_0 = -32^\circ47'35\overset{''}{.}08$ (J2000), coincident with the composite V4046 Sgr stellar position in the UCAC3 catalog (Zacharias et al. 2010). We adopted the distance inferred by Torres et al. (2006) from the kinematic parallax (moving cluster) technique, $d = 73$ pc (but see Section 5 regarding alternative values).

Some additional practical simplifications can be made, since the focus here is on the velocity field and not the disk structure details. Because the line opacity is so much greater than the dust opacity, the normalization parameters $X_{\rm co}$ and Σ_c are not independent: we can only constrain their product. In practice, we adopt a joint CO disk mass parameter, $M_{\rm co} = X_{\rm co}\Sigma_c(2\pi r_c^2)/(2-\gamma)$, for that purpose. Moreover, after extensive experimentation, we concluded that two more parameters should be fixed. First, we found that the disk orientation was very well determined (within 1°) at ${\rm PA}_d = 76^\circ$ (E of N), so that continued iteration on a more precise value was a waste of computational resources: fixing this parameter has negligible quantitative impact on the other model parameters or their uncertainties. And second, we fixed the surface density gradient, $\gamma = 1$. The key parameters that set the density profile, $\{\gamma, r_c\}$, are anti-correlated and strongly degenerate; statistically indistinguishable model fits can be found over a large range of these parameters. The degeneracy is remarkably narrow and could easily be missed with standard minimization algorithms (resulting in local χ^2 minima with misleadingly tight constraints on the gradient). Fortunately, this degeneracy has minimal impact on the parameters most relevant for characterizing the disk velocity field: the precision and accuracy of an M_* determination are not notably affected by the uncertainties in $\{\gamma, r_c\}$. With that in mind, we have made the modeling process more tractable with a fixed γ.

Making use of those simplifications, a synthetic CO spectral datacube can be calculated by specifying seven free parameters, $\{M_{\rm co}, r_c, T_{10}, q, \xi, i_d, \text{and } M_*\}$. That model datacube is then resampled at the observed velocities and spatial frequencies and processed in the same way as the data (see Section 2) to produce a set of synthetic spectral visibilities. Those model visibilities are evaluated with respect to the data by computing a composite χ^2 value, summed over the real and imaginary components in 25 spectral channels. The best-fit set of model parameters and their associated uncertainties were determined with a Monte Carlo Markov Chain (MCMC) technique, using the affine invariant ensemble sampler developed by Goodman & Weare (2010; see also Foreman-Mackey et al. 2012), using a jump probability $\propto e^{-\Delta\chi^2/2}$. To our knowledge, this is the first application of these more sophisticated MCMC methods for parameter estimation in this particular context: previous studies have relied on downhill simplex routines (e.g., Guilloteau & Dutrey 1998; Simon et al. 2000), sometimes with clever modifications to address asymmetric uncertainties (Piétu et al. 2007). Although comparatively the MCMC technique is computationally expensive, this Bayesian treatment has the distinct advantage of providing the posterior probability distributions for each parameter in the complex, multi-dimensional parameter-space of the underlying disk model.

4. RESULTS

The best-fit model derived from the SMA data is compiled in Table 1, which lists the mode (peak) of the posterior probability distribution for each parameter along with its uncertainty, based on the range of values that encompass 68% of the distribution area (i.e., 1σ uncertainties for a Gaussian distribution). Figure 3 makes a direct comparison between the data and the best-fit model in the spectral image plane, demonstrating the fit quality with only low-level (statistically insignificant) residuals present in the channel maps. The best-fit model has a reduced $\tilde{\chi}^2 = 967,427/977,000 = 0.9902$. A more detailed view of the multi-dimensional results of the modeling analysis is presented in Figure 4, where we have taken the 30,000 MCMC

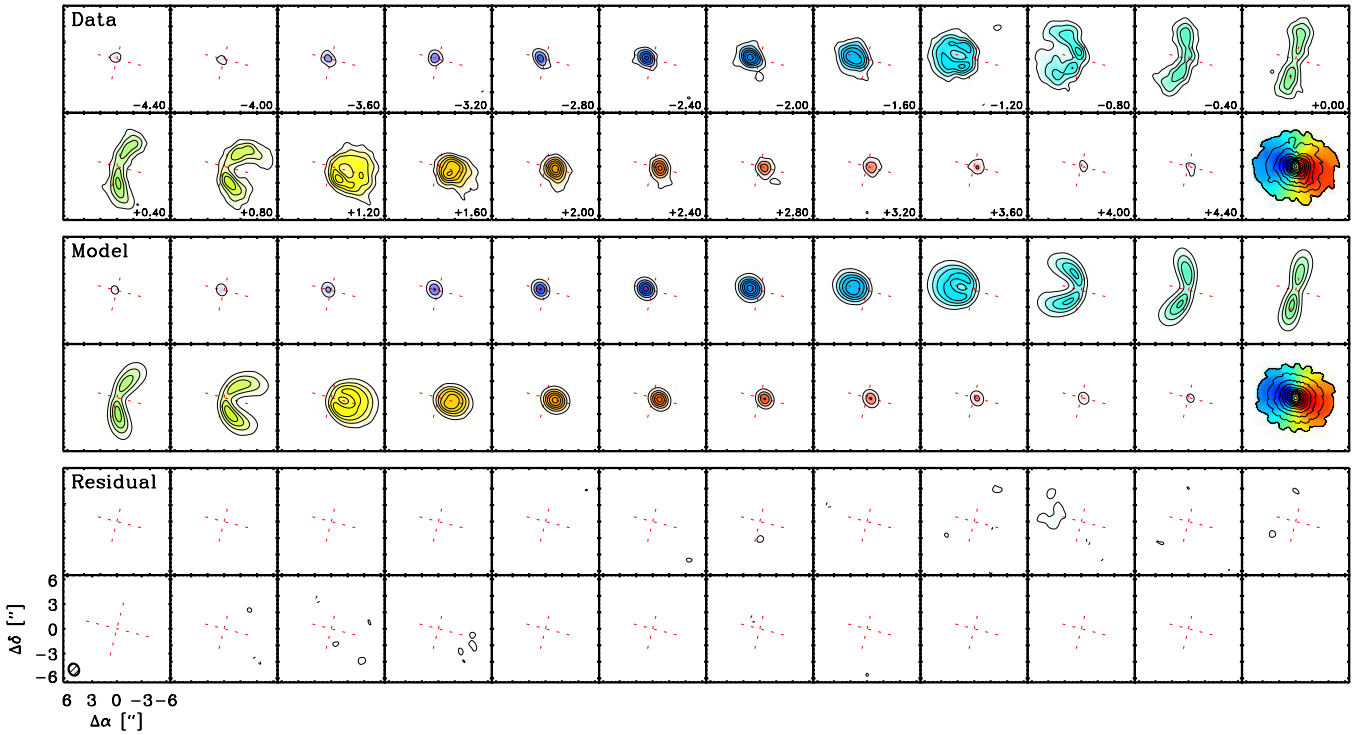

Figure 3. Channel maps of the CO $J = 2$–1 emission line from the SMA observations (top), the best-fit disk model (top), and the imaged residuals (bottom) with the channel velocity increasing from the top left to the bottom right. The last panel shows the zeroth (contours) and first (color scale) moment maps as in Figure 2. The best-fit model parameters are listed in Table 1.

(A color version of this figure is available in the online journal.)

Table 1
Disk Model Parameters

Parameter	Units	Estimate
$M_{\rm co}$	$(10^{-6}\ M_\odot)$	$2.8^{+3.7}_{-1.5}$
r_c	(AU)	45^{+5}_{-3}
q	...	0.63 ± 0.01
T_{10}	(K)	115 ± 5
ξ	(km s^{-1})	0.14 ± 0.01
i_d	(°)	$33.5^{+0.7}_{-1.4}$
M_*	$(M_\odot)$	$1.75^{+.09}_{-.06}$

Notes. See Section 3 for a description of the model parameters. The uncertainties for each parameter are determined from the width of the posterior distribution that encapsulates 68% of the models around the peak (equivalent to 1σ for Gaussian random variables.

samples computed and marginalized over parameter subsets to display one- and two-parameter posterior probability distributions. The marginalized distributions for individual parameters are single peaked, while the paired distributions highlight internal degeneracies in the model. For example, there are tight correlations between normalizations and sizes (e.g., $\{M_{\rm co}, r_c\}$, to conserve the integrated line intensity; this would be modified were γ a free parameter) or gradients (e.g., $\{T_{10}, q\}$, to maintain an appropriate temperature in the outer disk; Mundy et al. 1996; Andrews & Williams 2007), as well as more subtle associations among parameters related to line broadening (among r_c, T_{10}, and ξ; Guilloteau & Dutrey 1998; Hughes et al. 2011). The degeneracy of most interest here is the $\{M_*, i_d\}$ anti-correlation, which is a natural consequence of reproducing the observed line-of-sight velocity pattern, $v_{\rm obs} \propto v_k \sin i_d \propto \sqrt{M_*} \sin i_d$ (i.e., $M_* \propto 1/\sin^2 i_d$).

The best-fit model parameters that describe the V4046 Sgr disk structure are typical for young protoplanetary disks. The adopted (fixed) surface density gradient ($\gamma = 1$) and characteristic radius ($r_c = 45^{+5}_{-3}$ AU) lie near the median values for a survey of disk structures in the Ophiuchus region (Andrews et al. 2009, 2010); the temperature profile ($T_{10} = 115 \pm 5$ K, $q = 0.63 \pm 0.01$; and therefore vertical density distribution) and turbulent linewidth ($\xi = 0.14 \pm 0.01$ km s^{-1}) are comparable to those inferred from CO emission in other T Tauri disks (e.g., Guilloteau & Dutrey 1998; Piétu et al. 2007; Hughes et al. 2008, 2011). If we assume that the CO mass fraction found in dark clouds ($X_{\rm co} \approx 10^{-4}$) is also applicable in the disk, the molecular density normalization parameter $M_{\rm co}$ implies a modest gas mass, $2.8^{+3.7}_{-1.5} \times 10^{-2}\ M_\odot$, validating a posteriori our assumption that self-gravity is negligible ($M_d/M_* \approx 10^{-2} \ll 1$). In any case, our simple treatment of the disk structure is really only used as a means to an end: the focus here is to place a firm constraint on the key parameter that determines the behavior of the disk velocity field—the central stellar mass, M_*.

We infer a total stellar mass of $M_* = 1.75^{+0.09}_{-0.06}\ M_\odot$ for the V4046 Sgr spectroscopic binary, a formally precise constraint with a relative uncertainty of 3%–5%. Figure 4 demonstrates that this estimate of M_* is essentially independent of the disk structure parameters in the model. The sole relevant degeneracy is with the disk inclination, which we infer to be $i_d = 33.^\circ5^{+0.7}_{-1.4}$ (a relative precision of ~2%–5%). Within the quoted uncertainties, these $\{M_*, i_d\}$ values are consistent with the previous determinations by Rodriguez et al. (2010), who used a simple χ^2 grid search and an altogether different underlying disk structure model. These $\{M_*, i_d\}$ measurements based on the circumstellar gas disk kinematics can be directly compared with the joint (degenerate) constraints on $\{M_*, i_*\}$ imposed by RV measurements of the spectroscopic binary itself. Although

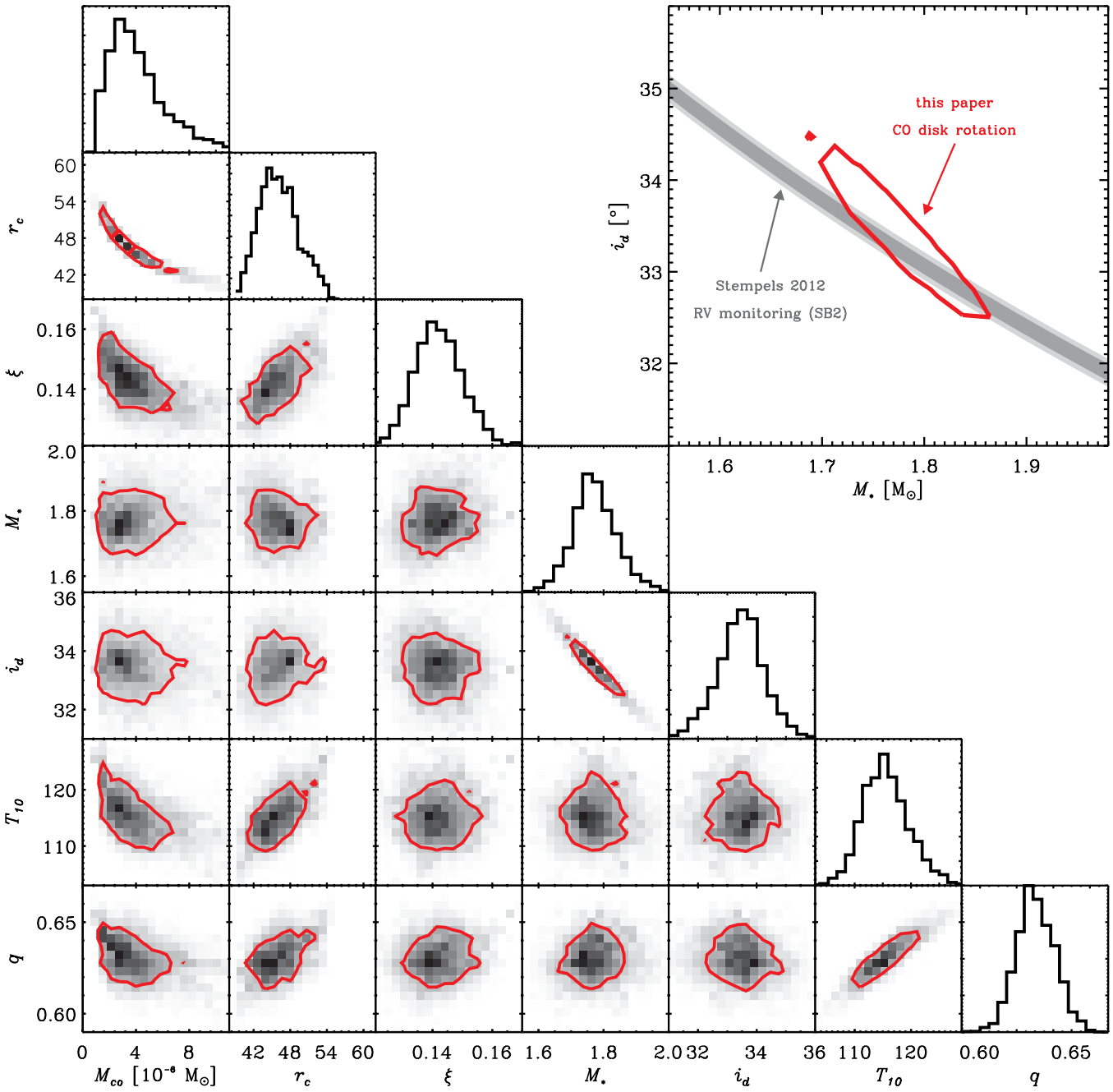

Figure 4. Marginalized parameters of the sampled posterior distribution. The 68% confidence contour is given by the red contour with each binned distribution shown by the linear gray scale.

(A color version of this figure is available in the online journal.)

various groups have studied this SB2 system (Quast et al. 2000; Stempels & Gahm 2004; Donati et al. 2011), by far the most robust constraints on the stellar parameters come from the long-term, extensive, and high resolution optical spectroscopic monitoring campaign conducted by H. C. Stempels (2012, in preparation). In that work, the RV data are found to be best explained with a binary that has a total mass $M_*(\sin i_*)^3 = 0.2923 \pm 0.0007\ M_\odot$. The inset in Figure 4 confirms that our disk kinematics constraints and the RV constraints by H. C. Stempels (2012, in preparation) coincide in the stellar-mass–inclination plane: the two *completely independent* methods find the same results well within their formal 1σ uncertainties. Adopting our best estimate of M_* and propagating the relevant uncertainties, the RV constraints suggest that $i_* = 33.^\circ42 \pm 0.01$. Therefore, we quantitatively confirm the finding of Rodriguez et al. (2010): the V4046 Sgr spectroscopic binary and its associated, large-scale circumbinary disk are co-planar within $|i_d - i_*| \approx 0.^\circ1 \pm 1^\circ$ across ~4 orders of magnitude in radial scale.

5. DISCUSSION

We have presented spatially and spectrally resolved SMA observations of the ^{12}CO $J = 2$–1 line emission from the isolated, nearby, and gas-rich circumstellar disk that orbits the close, pre-MS SB2 V4046 Sgr. Adopting a simple parametric model for the structure of a flared Keplerian disk, we employ an MCMC technique to infer the properties of the disk velocity field from these data and thereby provide a robust statistical

estimate for the total mass of the central binary. We find that these CO line data are best reproduced for a binary mass $M_* = 1.75^{+0.09}_{-0.06}\,M_\odot$ and a disk viewing angle inclined by $i_d = 33.^\circ5^{+0.7}_{-1.4}$ from face-on. Those values are in excellent agreement with the completely independent inferences of H. C. Stempels (2012, in preparation), made from his extensive RV monitoring campaign of the spectroscopic binary itself. The orbital planes of the binary ($a = 0.045$ AU) and its associated circumbinary disk (on radial scales out to ∼400 AU) are aligned within $\sim 0.^\circ1 \pm 1^\circ$. These results demonstrate that, despite its complexity, the disk-based kinematic method for estimating the masses of young stars is both *precise* (at the level of a few percent) and *accurate* in an absolute sense, as verified here by an entirely independent dynamical constraint.

The disk-based dynamical estimate of M_* can be combined with the RV constraints of H. C. Stempels (2012, in preparation) and other information from the literature to assess the predictions of pre-MS stellar evolution models. Coupling our M_* estimate with the stellar mass ratio (q) and mass function ($M_*(\sin i_*)^3$) determined by Stempels, we can derive the masses of the individual stellar components in the V4046 Sgr binary, 0.90 ± 0.05 and $0.85 \pm 0.04\,M_\odot$, and their orbital inclination, $i_* = 33.^\circ42 \pm 0.01$.[4] Assuming that the stellar rotation axes are aligned with the binary orbital axis (a spin–orbit alignment presumably induced by tides in this close, circularized system; e.g., Zahn 1977; Hut 1981; Melo et al. 2001), the radial and *rotational* velocities measured for each stellar component by Stempels can be used to determine the stellar radii, 1.25 ± 0.04 and $1.21 \pm 0.04\,R_\odot$. Stempels & Gahm (2004) inferred spectral types of K5 and K7 in this system, corresponding to effective temperatures of 4350 ± 240 and 4060 ± 210 K for the standard conversion advocated by Schmidt-Kaler (1982); an ambiguity of one spectral subclass has been assumed to estimate the temperature uncertainties. Those measurements imply that the individual stellar luminosities are 0.50 ± 0.11 and $0.36 \pm 0.08\,L_\odot$ (a total luminosity of $0.86 \pm 0.14\,L_\odot$).

Figure 5 shows the composite optical/near-infrared spectrum expected from the V4046 Sgr binary, given the effective temperatures, stellar radii, and masses derived above from the combination of RV data and our disk-based measurements (black curve, with uncertainty in shaded gray). This spectral energy distribution prediction was generated from an interpolated grid of Lejeune et al. (1997) model spectra, assuming the appropriate stellar gravities ($\log g = 4.20 \pm 0.02$ in both cases), negligible interstellar reddening ($A_V = 0$), and our adopted $d = 73$ pc. Representative broadband photometric data are marked as the data points in Figure 5, constructed from the weighted mean magnitudes of Hutchinson et al. (1990), Strassmeier et al. (1993), Jensen & Mathieu (1997), and the Two Micron All Sky Survey (Skrutskie et al. 2006) and DENIS (Epchtein et al. 1997) surveys: uncertainties were taken as the quadrature sum of the standard deviation of the weighted mean and the maximal deviation from the weighted mean, in an effort to more faithfully represent potential uncertainties due to variability. A quick examination of Figure 5 demonstrates that the spectral morphology of the data and model prediction are a good match, although the normalizations appear discrepant. Scaling the (best-fit) predicted spectrum down by ∼30%±15% provides a good match to the observed spectrum; a composite luminosity of $0.60 \pm 0.13\,L_\odot$ is more appropriate (red curve). Therefore,

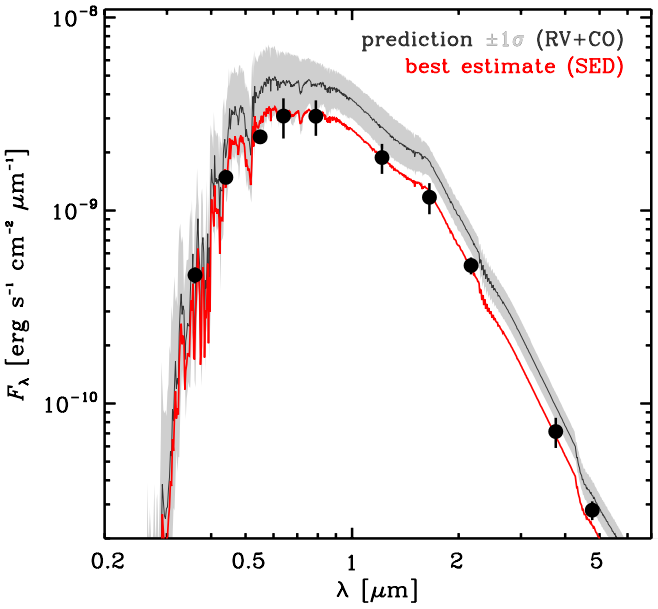

Figure 5. Composite optical/near-infrared broadband spectrum observed for the V4046 Sgr binary (see the text for references and discussion of uncertainties), along with a model spectrum predicted from a combination of the CO rotation curve analysis in Section 4 and the optical spectroscopic monitoring campaign of H. C. Stempels (2012, in preparation) (black curve, with uncertainties shaded in gray). The red curve corresponds to that prediction scaled down by ∼30% in luminosity, to best reproduce the observations. The data and the predictions are marginally discrepant (1.4σ) in terms of their normalization; potential causes of that minor difference are discussed in the text.

(A color version of this figure is available in the online journal.)

the predicted and observed composite binary luminosities are marginally ($\sim 1.4\sigma$) different.

Although formally the conflict in these luminosity values is not statistically significant, it is still interesting to consider some potential paths for a better reconciliation of all the data. Perhaps the most straightforward means of doing so is to modify the assumed distance to the system: taken at face value, a ∼30% increase to $d \approx 95$ pc implies an inherently more luminous pair of stars with a spectrum that would be in good agreement with the observations. However, that same re-normalization impacts the total stellar mass inferred from the CO data, with a linear scaling to $M_* \approx 2.3\,M_\odot$ that introduces a substantial ($\sim 2\sigma$) discrepancy in the $\{M_*, i\}$-plane between the disk-kinematics and RV techniques for estimating stellar parameters. Although it hardly seems worthwhile to trade one marginal discrepancy for another (which is technically less marginal), there is no a priori reason that the orbital planes of the disk and binary need to be aligned with the precision inferred in Section 4. Unfortunately, little guidance is provided in the form of an uncertainty on the kinematic parallax measurement of Torres et al. (2006). In any case, discrepancies in effective temperatures and luminosities are not necessarily uncommon for active young stars (Stassun et al. 2012), and particularly for those in close binary systems (e.g., Goméz Maqueo Chew et al. 2012).

Ultimately, dwelling on a marginal luminosity discrepancy is not well justified, especially given the independent distance estimate from the Torres et al. (2006) study. In the following, we adopt the stellar parameters inferred from the joint constraints of the CO disk spatio-kinematics and the optical RV studies of Stempels assuming $d = 73$ pc, but use individual stellar luminosities scaled down by 30% to best match the observed optical and near-infrared spectrum: $0.35 \pm 0.10\,L_\odot$ and $0.25 \pm$

[4] Here and throughout, we conservatively adopt the larger of all asymmetric uncertainties for simplicity.

Table 2
Comparison with pre-MS Evolution Models

	V4046 Sgr A				V4046 Sgr B			
	M_* ($M_\odot$)		t_* (Myr)		M_*		t_*	
Models	H-R	+dyn	H-R	+dyn	H-R	+dyn	H-R	+dyn
DM98	$0.84^{+0.06}_{-0.10}$	$0.88^{+0.03}_{-0.05}$	6^{+27}_{-1}	9^{+10}_{-2}	$0.76^{+0.06}_{-0.09}$	$0.82^{+0.03}_{-0.05}$	8^{+19}_{-1}	11^{+8}_{-3}
BCAH98	$0.89^{+0.09}_{-0.12}$	$0.90^{+0.04}_{-0.06}$	10^{+37}_{-1}	18^{+10}_{-9}	$0.80^{+0.07}_{-0.09}$	$0.84^{+0.04}_{-0.05}$	10^{+14}_{-1}	13^{+12}_{-10}
SDF00	$0.83^{+0.13}_{-0.06}$	$0.88^{+0.05}_{-0.05}$	12^{+52}_{-1}	20^{+31}_{-8}	$0.75^{+0.09}_{-0.10}$	$0.83^{+0.04}_{-0.05}$	11^{+39}_{-2}	16^{+13}_{-4}
TPD11	$0.86^{+0.09}_{-0.11}$	$0.89^{+0.04}_{-0.05}$	9^{+35}_{-1}	14^{+10}_{-5}	$0.78^{+0.07}_{-0.11}$	$0.85^{+0.04}_{-0.04}$	9^{+21}_{-1}	12^{+10}_{-3}
⟨mean⟩	$0.84^{+0.11}_{-0.08}$	$0.89^{+0.04}_{-0.05}$	9^{+43}_{-1}	12^{+17}_{-3}	$0.77^{+0.08}_{-0.11}$	$0.83^{+0.04}_{-0.05}$	10^{+10}_{-3}	13^{+11}_{-3}

Notes. Stellar mass and age estimates from the four different pre-MS evolution models are calculated using the H-R observables $\{\log L, \log T\}$, following the methods outlined in Section 5. We report results for both a uniform (H-R) and Gaussian (+dyn) prior on the mass, with the latter based on the dynamical constraints. The mean values are computed for all the models, following the technique outlined by Hoeting et al. (1999).

0.08 $L_\odot$ (note that each component is slightly less luminous than reported by Donati et al. 2011). With those results, we can make comparisons with the predictions of pre-MS evolution models to estimate the ages (t_*) and masses of the individual stars in the V4046 Sgr binary. To accomplish that we follow the Bayesian methodology of Jørgensen & Lindegren (2005), which employs a finely interpolated grid of pre-MS models in the H-R diagram to estimate the probability distributions of stellar mass and age given the measured values (and uncertainties) of effective temperatures and luminosities (see also Gennaro et al. 2012). If we define the observables as $\{x, y\} = \{\log T, \log L\}$ with associated uncertainties $\{\sigma_x, \sigma_y\}$ and the pre-MS model predictions $\{\hat{x}(M_*, t_*), \hat{y}(M_*, t_*)\}$, we can write the likelihood function as a multivariate Gaussian,

$$\mathcal{L}(\hat{x}, \hat{y}|x, y) = \frac{1}{2\pi\sigma_x\sigma_y} \exp\left\{-\frac{1}{2}\left[\frac{(x-\hat{x})^2}{\sigma_x^2} + \frac{(y-\hat{y})^2}{\sigma_y^2}\right]\right\}. \quad (12)$$

The best-fit $\{M_*, t_*\}$ are then directly determined from the $\{\hat{x}, \hat{y}\}$ that maximize the likelihood, with uncertainties that can be calculated from the shape of the likelihood distribution. This procedure was conducted for four different pre-MS evolution models, assuming solar composition, a fractional deuterium abundance of 2×10^{-5}, and a convective mixing parameter $\alpha \approx 1.7$–2.0: D'Antona & Mazzitelli (1998), Baraffe et al. (1998), Siess et al. (2000), and Tognelli et al. (2011).

The results of these comparisons are presented in Table 2. Figure 6 shows the V4046 Sgr stellar properties that were inferred from each of the four reference sets of pre-MS evolutionary model tracks in the H-R diagram. All of the evolutionary models make predictions for the V4046 Sgr stellar masses that are remarkably consistent with each other and the dynamical masses inferred in Section 4. The stellar masses that formally maximize the likelihood in Equation (12) are systematically ∼2%–10% below the best-fit dynamical masses, an underprediction typical of pre-MS models regardless of the dynamical method used to estimate M_* (Hillenbrand & White 2004; Gennaro et al. 2012). However, those modest discrepancies are not statistically significant, given the uncertainties on $\{L, T\}$ and the dynamical masses. An examination of Figure 6 demonstrates that the V4046 Sgr stars are nearly evolved off the Hayashi track, having presumably developed radiative cores as expected for their solar-like masses. The clear implication of their location in the H-R diagram is that the V4046 Sgr binary is comparatively *old* for a pre-MS system, as has been previously reported by Donati et al. (2011) and Kastner et al. (2011). The models used here suggest that a large range of ages are plausible, from ∼5 to 30 Myr, and confirm that the binary components are coeval. If we include a Gaussian prior representing the dynamical masses into the Bayesian analysis of the H-R diagrams described above (labeled as "+dyn" in Table 2), we can infer a smaller range of acceptable "dynamical" ages from each set of pre-MS models. The different pre-MS model predictions with these dynamical priors are shown together, and averaged (weighted by the posterior probability for each model; Hoeting et al. 1999), in Figure 7: the averaged results suggest ages of 12^{+17}_{-3} and 13^{+11}_{-3} Myr for V4046 Sgr A and B, respectively. The corresponding coeval age is 13^{+8}_{-3} Myr, in good agreement with the age constraints from the putative far-flung companion(s) V4046 Sgr C[D] (at a separation of ∼12,350 AU or 2.″8 on the sky; Kastner et al. 2011).

Torres et al. (2006) suggested that the observed space motion of V4046 Sgr is consistent with a high probability of membership in the β Pic moving group, a widespread and local ($d \approx 34 \pm 21$ pc) stellar association with an age range estimated to be ∼8–20 Myr (e.g., Zuckerman et al. 2001; Zuckerman & Song 2004; Torres et al. 2008). The kinematic parallax calculated by Torres et al. ($d \approx 73$ pc) and component ages estimated here for the V4046 Sgr binary are certainly supportive of that conclusion. If that is the case, it is worth noting the uniqueness of the V4046 Sgr circumstellar environment: there are no other β Pic moving group members that are known to host such a massive, long-lived, gas-rich accretion disk. Regardless of its original association, the proximity and advanced age of V4046 Sgr make for a remarkable case study in both the long-term evolution of protoplanetary disk structure and the fundamental properties of pre-MS binary stars.

Although V4046 Sgr is a particularly striking example of the methodology behind disk-based dynamical estimates of stellar masses, we anticipate that these techniques will find considerably more use in the near future as the Atacama Large Millimeter Array (ALMA) project is completed. Even with vastly improved data quality, this simplified model to extract the gas disk rotation curve from such interferometric observations (see Section 3) remains complex. However, we have demonstrated that the method is robust, accurate, and precise, by using independent dynamical constraints from the V4046 Sgr spectroscopic binary RV monitoring results. In practice, these constraints and others like them (notably for UZ Tau E; see Simon et al. 2000; Prato et al. 2002) effectively serve as a check on the absolute calibration of the modeling technique described in

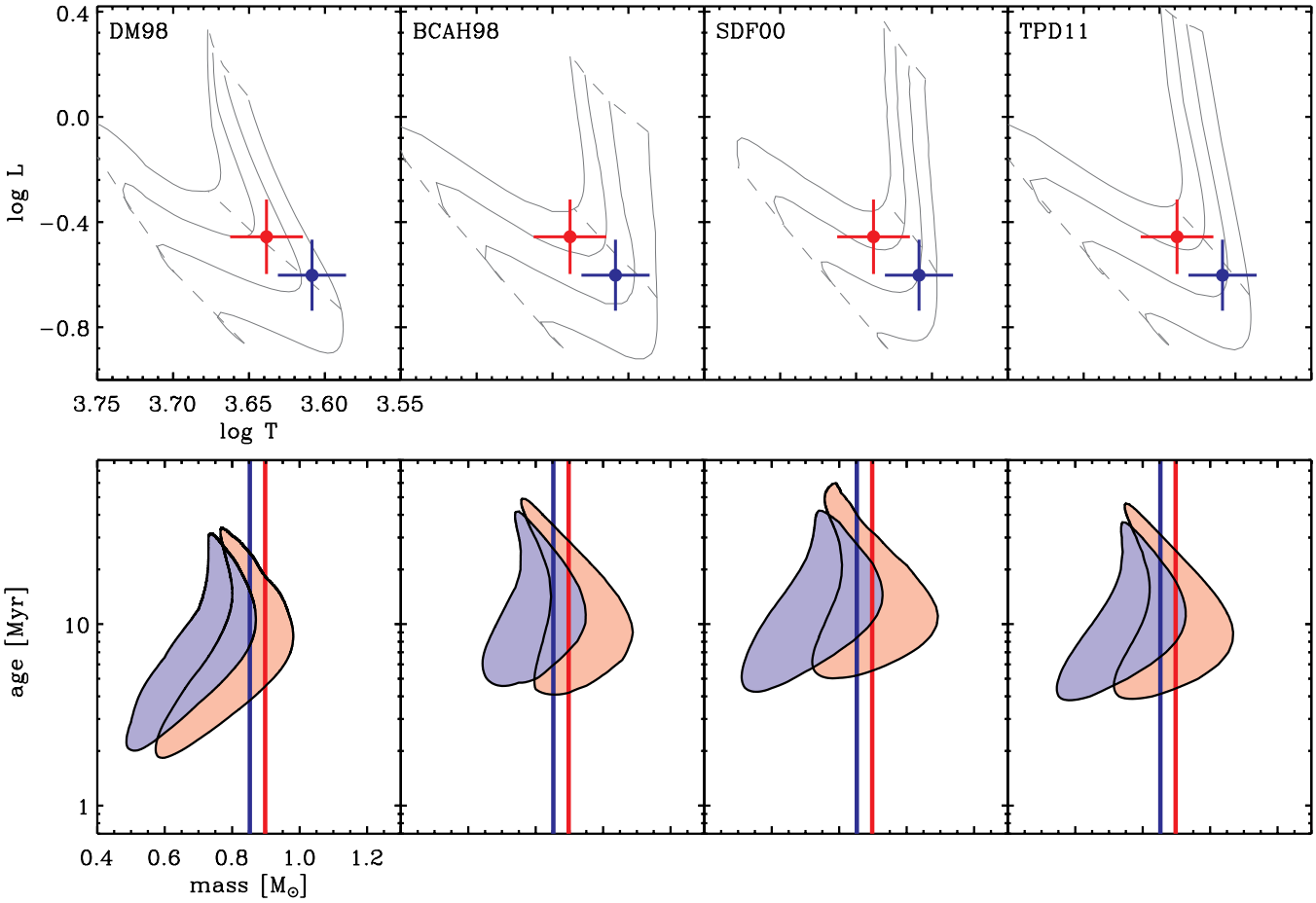

Figure 6. Top: the V4046 Sgr stellar properties (primary in red, secondary in blue) compared with the pre-MS evolutionary models of (from left to right) D'Antona & Mazzitelli (DM98), Baraffe et al. (BCAH98), Siess et al. (SDF00), and Tognelli et al. (2011; TPD11) in the H-R diagram. In each case, the mass tracks for $M_* = \{0.7, 0.8, 0.9, 1.0\}$ $M_\odot$ are shown as gray solid curves, with isochrones for $t_* = \{1, 10, 100\}$ Myr denoted as gray dashed curves. Bottom: the 68% confidence intervals for the posterior likelihood distribution in the $\{M_*, t_*\}$-plane derived from the H-R diagram for each model type, using the Bayesian methodology of Jørgensen & Lindegren (2005). The vertical lines indicate the individual stellar masses as determined by combining the total mass from the disk analysis in Section 4 and the mass ratio derived from the spectroscopic analysis of H. C. Stempels (2012, in preparation).

(A color version of this figure is available in the online journal.)

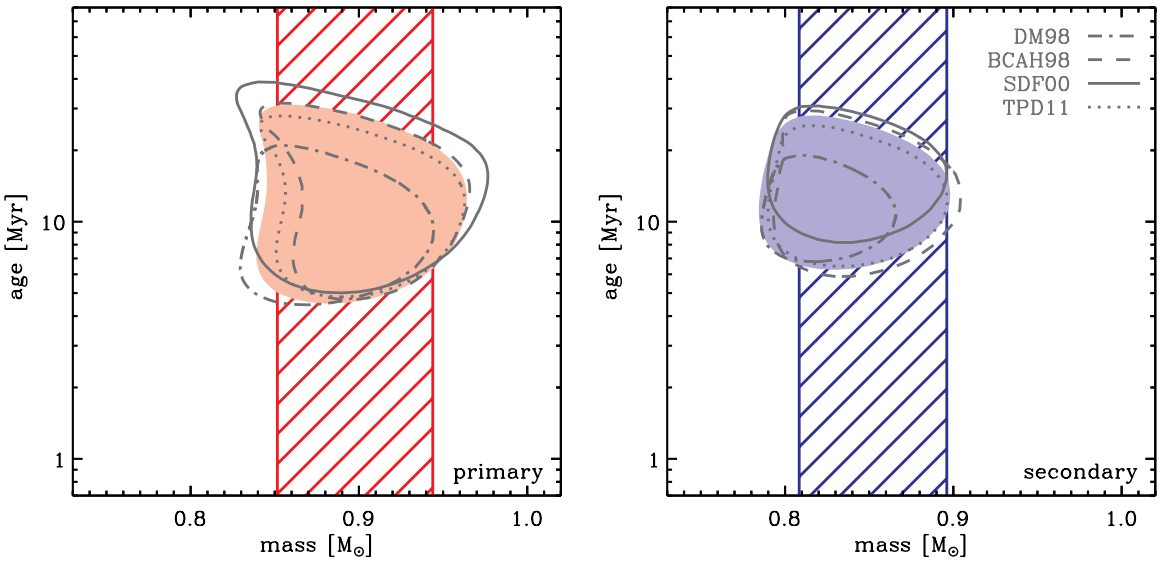

Figure 7. 68% confidence intervals for the posterior likelihood distribution in the $\{M_*, t_*\}$-plane derived from the H-R diagram for each model type (see key in the right panel) overlaid together on the individual V4046 Sgr components (left primary; right secondary), now assuming the dynamical masses determined in Section 4 as Gaussian priors (the "+dyn" models references in Table 2). The filled shaded region corresponds to the averaged likelihoods from the four different pre-MS models. The dynamical masses and their uncertainties are marked as a hatched, shaded vertical column.

(A color version of this figure is available in the online journal.)

Section 3. The consistency between the independent dynamical constraints on the V4046 Sgr stellar masses validates the application of this procedure to dynamically "weigh" single, isolated pre-MS stars based on their gas disk kinematics. Along with an investment in accurate stellar luminosity and temperature measurements, ALMA observations of the molecular gas kinematics in circumstellar disks will usher in a new era of precision in the fundamental astrophysical properties of young stars.

6. SUMMARY

We have presented sensitive, high-resolution SMA observations of the ^{12}CO $J = 2$–1 line emission from the massive, gas-rich disk orbiting the SB2 star V4046 Sgr. Using simple radiation transfer calculations for a disk structure model with a Keplerian velocity field, we fit the observed spectral visibilities using a stochastic model optimization technique that simultaneously infers model parameter values and their uncertainties. Our specific focus has been on the key model parameters that describe the disk velocity field, with a goal of placing a firm, dynamical constraint on the mass of the central binary. The key conclusions of our analysis are as follows.

1. From modeling the CO line emitted by the circumbinary disk, we infer that the total stellar mass of the V4046 Sgr binary is $M_* = 1.75^{+0.09}_{-0.06}\,M_\odot$, assuming the kinematic parallax distance of 73 pc estimated by Torres et al. (2006). That measurement is in excellent agreement with the independent dynamical constraints imposed from the analysis of an optical spectroscopic monitoring campaign of the RV variations from the binary itself (H. C. Stempels 2012, in preparation).
2. The mutual consistency of these distinct dynamical constraints on the stellar masses verifies that the mass determination based on the velocity field of the disk gas is accurate in an absolute sense, as well as remarkably precise (with a 3%–5% formal uncertainty on M_*).
3. That same combination of constraints from millimeter and optical spectroscopic measurements confirms that the orbital planes of the stars and their accompanying circumbinary disk are coplanar, with inferred inclination angles ($i_d = 33.^\circ5^{+0.7}_{-1.4}$ and $i_* = 33.^\circ4 \pm 0.01$) that differ by $0.^\circ1 \pm 1^\circ$ over roughly four decades in radius, from $\sim$0.04 to 400 AU.
4. The inferred component masses of the V4046 Sgr binary are in uniformly good agreement with a variety of pre-MS evolution model predictions. When combined with our dynamical constraints, those same models confirm the coevality of the binary components and suggest an average age for the system of 13^{+8}_{-3} Myr. Therefore, V4046 Sgr hosts one of the oldest and nearest gas-rich primordial accretion disks currently known.

We are very grateful to Joel Kastner, Guillermo Torres, and Zachory Berta for some insightful discussions and suggestions, as well as to Germano Quast for being kind enough to provide additional information on their optical observations of the V4046 Sgr binary. The SMA is a joint project between the Smithsonian Astrophysical Observatory and the Academia Sinica Institute of Astronomy and Astrophysics and is funded by the Smithsonian Institution and the Academia Sinica.

REFERENCES

Alibert, Y., Mordasini, C., & Benz, W. 2011, A&A, 526, 63
Andrews, S. M., & Williams, J. P. 2007, ApJ, 659, 705
Andrews, S. M., Wilner, D. J., Hughes, A. M., Qi, C., & Dullemond, C. P. 2009, ApJ, 700, 1502
Andrews, S. M., Wilner, D. J., Hughes, A. M., Qi, C., & Dullemond, C. P. 2010, ApJ, 723, 1241
Artymowicz, P., & Lubow, S. H. 1994, ApJ, 421, 651
Baraffe, I., & Chabrier, G. 2010, A&A, 521, 44
Baraffe, I., Chabrier, G., Allard, F., & Hauschildt, P. H. 1998, A&A, 337, 403
Baraffe, I., Chabrier, G., Allard, F., & Hauschildt, P. H. 2002, A&A, 382, 563
Baraffe, I., Chabrier, G., & Gallardo, J. 2009, ApJ, 702, L27
Bastian, N., Covey, K. R., & Meyer, M. R. 2010, ARA&A, 48, 339
Beckwith, S. V. W., & Sargent, A. I. 1993, ApJ, 402, 280
Beckwith, S. V. W., Sargent, A. I., Chini, R. S., & Güsten, R. 1990, AJ, 99, 924
Boden, A. F., Akeson, R. L., Sargent, A. I., et al. 2009, ApJ, 696, L111
Boden, A. F., Sargent, A. I., Akeson, R. L., et al. 2005, ApJ, 635, 442
Boden, A. F., Torres, G., Duchêne, G., et al. 2012, ApJ, 747, 17
Boden, A. F., Torres, G., Sargent, A. I., et al. 2007, ApJ, 670, 1214
Byrne, P. B. 1986, Ir. Astron. J., 17, 294
D'Alessio, P., Canto, J., Calvet, N., & Lizano, S. 1998, ApJ, 500, 411
D'Antona, F., & Mazzitelli, I. 1998, in ASP Conf. Ser. 134, Brown Dwarfs and Extrasolar Planets, ed. R. Rebolo, E. L. Martin, & M. R. Z. Osorio (San Francisco, CA: ASP), 442
D'Antona, F., Ventura, P., & Mazzitelli, I. 2000, ApJ, 543, L77
Dartois, E., Dutrey, A., & Guilloteau, S. 2003, A&A, 399, 773
Donati, J.-F., Gregory, S. G., Montmerle, T., et al. 2011, MNRAS, 417, 1747
Duchêne, G., Beust, H., Adjali, F., Konopacky, Q. M., & Ghez, A. M. 2006, A&A, 457, L9
Dutrey, A., Guilloteau, S., Prato, L., et al. 1998, A&A, 338, L63
Dutrey, A., Guilloteau, S., & Simon, M. 1994, A&A, 286, 149
Epchtein, N., et al. 1997, Messenger, 87, 27
Foreman-Mackey, D., Hogg, D. W., Lang, D., & Goodman, J. 2012, arXiv:1202.3665
Gennaro, M., Prada Moroni, P. G., & Tognelli, E. 2012, MNRAS, 420, 986
Goodman, J., & Weare, J. 2010, Comm. App. Math. Comp. Sci., 5, 65
Goméz Maqueo Chew, Y., Stassun, K. G., Prša, A., et al. 2012, ApJ, 745, 58
Guilloteau, S., & Dutrey, A. 1998, A&A, 339, 467
Hartmann, L., Calvet, N., Gullbring, E., & D'Alessio, P. 1998, ApJ, 495, 385
Hillenbrand, L. A., & White, R. J. 2004, ApJ, 604, 741
Ho, P. T. P., Moran, J. M., & Lo, K. Y. 2004, ApJ, 616, L1
Hoeting, J. A., Madigan, D., Raftery, A. E., & Volinsky, C. T. 1999, Statist. Sci., 14, 4
Hughes, A. M., Wilner, D. J., Andrews, S. M., Qi, C., & Hogerheijde, M. R. 2011, ApJ, 727, 85
Hughes, A. M., Wilner, D. J., Qi, C., & Hogerheijde, M. R. 2008, ApJ, 678, 1119
Hut, P. 1981, A&A, 99, 126
Hutchinson, M. G., Evans, A., Winkler, H., & Spencer Jones, J. 1990, A&A, 234, 230
Isella, A., Testi, L., Natta, A., et al. 2007, A&A, 469, 213
Jensen, E. L. N., & Mathieu, R. D. 1997, AJ, 114, 301
Jørgensen, B. R., & Lindegren, L. 2005, A&A, 436, 127
Kastner, J. H., Sacco, G. G., Montez, R., et al. 2011, ApJ, 740, L17
Kastner, J. H., Zuckerman, B., Hily-Blant, P., & Forveille, T. 2008, A&A, 492, 469
Koerner, D. W., Sargent, A. I., & Beckwith, S. V. W. 1993, Icarus, 106, 2
Lejeune, T., Cuisinier, F., & Buser, R. 1997, A&AS, 125, 229
Lynden-Bell, D., & Pringle, J. E. 1974, MNRAS, 168, 603
Mathieu, R. D., Adams, F. C., & Latham, D. W. 1991, AJ, 101, 2184
Mathieu, R. D., Stassun, K., Basri, G., et al. 1997, AJ, 113, 1841
Mathieu, R. D., Walter, F. A., & Myers, P. C. 1989, AJ, 98, 987
Melo, C. H. F., Covino, E., Alcalá, J. M., & Torres, G. 2001, A&A, 378, 898
Mendes, L. T. S., D'Antona, F., & Mazzitelli, I. 1999, A&A, 341, 174
Morales-Calderón, M., Stauffer, J. R., Stassun, K. G., et al. 2012, ApJ, 753, 149
Mundy, L. G., Looney, L. W., Erickson, W., et al. 1996, ApJ, 464, L169
Öberg, K. I., Qi, C., Fogel, J. K. J., et al. 2011, ApJ, 734, 98
Pavlyuchenkov, Y., Semenov, D., Henning, T., et al. 2007, ApJ, 669, 1262
Piétu, V., Dutrey, A., & Guilloteau, S. 2007, A&A, 467, 163
Prato, L., Simon, M., Mazeh, T., Zucker, S., & McLean, I. S. 2002, ApJ, 579, L99
Quast, G. R., Torres, C. A. O., de La Reza, R., da Silva, L., & Mayor, M. 2000, in IAU Symp. 200, Birth and Evolution of Binary Stars, Poster, ed. B. Reipurth & H. Zinnecker (Cambridge: Cambridge Univ. Press), 28P
Rodriguez, D. R., Kastner, J. H., Wilner, D., & Qi, C. 2010, ApJ, 720, 1684
Schaefer, G. H., Simon, M., Beck, T. L., Nelan, E., & Prato, L. 2006, AJ, 132, 2618
Schaefer, G. H., Simon, M., Nelan, E., & Holfeltz, S. T. 2003, AJ, 126, 1971
Schaefer, G. H., Simon, M., Prato, L., & Barman, T. 2008, AJ, 135, 1659

Schmidt-Kaler, T. 1982, in Landölt Bornstein, Group VI, Vol. 2, ed. K.-H. Hellwege (Berlin: Springer), 454
Schöier, F. L., van der Tak, F. F. S., van Dishoeck, E. F., & Black, J. H. 2005, A&A, 432, 369
Siess, L., Dufour, E., & Forestini, M. 2000, A&A, 358, 593
Siess, L., Forestini, M., & Dougados, C. 1997, A&A, 326, 1001
Siess, L., & Livio, M. 1997, ApJ, 490, 785
Simon, M., Dutrey, A., & Guilloteau, S. 2000, ApJ, 545, 1034
Skrutskie, M. F., Cutri, R. M., Stiening, R., et al. 2006, AJ, 131, 1163
Stassun, K. G., Kratter, K. M., Scholz, A., & Dupuy, T. J. 2012, ApJ, 756, 47
Stassun, K. G., Mathieu, R. D., Vaz, L. P. R., Stroud, N., & Vrba, F. J. 2004, ApJS, 151, 357
Steffen, A. T., Mathieu, R. D., Lattanzi, M. G., et al. 2001, AJ, 122, 997
Stempels, H. C., & Gahm, G. F. 2004, A&A, 421, 1159
Strassmeier, K. G., Hall, D. S., Fekel, F. C., & Scheck, M. 1993, A&AS, 100, 173
Tamazian, V. S., Docobo, J. A., White, R. J., & Woitas, J. 2002, ApJ, 578, 925
Tognelli, E., Prada Moroni, P. G., & Degl'Innocenti, S. 2011, A&A, 533, A109
Torres, C. A. O., Quast, G. R., da Silva, L., et al. 2006, A&A, 460, 695
Torres, C. A. O., Quast, G. R., Melo, C. H. F., & Sterzik, M. F. 2008, Handbook of Star Forming Regions (Vol. II; San Francisco, CA: ASP), 757
Zacharias, N., Finch, C., Girard, T., et al. 2010, AJ, 139, 2184
Zahn, J.-P. 1977, A&A, 57, 383
Zuckerman, B., & Song, I. 2004, ARA&A, 42, 685
Zuckerman, B., Song, I., Bessell, M. S., & Webb, R. A. 2001, ApJ, 562, L87